

Size, Shape, and Lateral Correlation of Highly Uniform, Mesoscopic, Self-Assembled Domains of Fluorocarbon–Hydrocarbon Diblocks at the Air/Water Interface: A GISAXS Study**

Mariam Veschgini^{+, [a]}, Wasim Abuillan^{+, [a]}, Shigeto Inoue^{+, [a, e]}, Akihisa Yamamoto^{+, [b]},
Salomé Mielke^{+, [a]}, Xianhe Liu^{+, [c]}, Oleg Konovalov^{+, [d]}, Marie Pierre Krafft^{+, [c]} and
Motomu Tanaka^{+, [a, b]}

The shape and size of self-assembled mesoscopic surface domains of fluorocarbon–hydrocarbon (*FnHm*) diblocks and the lateral correlation between these domains were quantitatively determined from grazing incidence small-angle X-ray scattering (GISAXS). The full calculation of structure and form factors unravels the influence of fluorocarbon and hydrocarbon block lengths on the diameter and height of the domains, and provides the inter-domain correlation length. The diameter of the domains, as determined from the form factor analysis, exhibits a monotonic increase in response to the systematic lengthening

of each block, which can be attributed to the increase in van der Waals attraction between molecules. The pair correlation function in real space calculated from the structure factor implies that the inter-domain correlation can reach a distance that is over 25 times larger than the domain's size. The full calculation of the GISAXS signals introduced here opens a potential towards the hierarchical design of mesoscale domains of self-assembled small organic molecules, covering several orders of magnitude in space.

1. Introduction

Semi-fluorinated alkanes, $C_nF_{2n+1}C_mH_{2m+1}$ (*FnHm* diblocks) are based on a covalent connection of fluorocarbon (*Fn*) and hydrocarbon (*Hm*) segments (Figure 1 a). Fluorocarbons and hydrocarbons are highly incompatible and differ significantly in many structural and physicochemical properties.^[1–2] For exam-

ple, fluorocarbon chains have a larger cross-sectional area ($\approx 27\text{--}30 \text{ \AA}^2$) than hydrocarbon chains ($\approx 18\text{--}21 \text{ \AA}^2$) and take a 15/7 helical conformation due to the larger steric requirements of fluorine. This results in a rigid rod-like *Fn* chain, in contrast to a planar hydrocarbon chain, which takes an *all-trans* conformation.^[3] Moreover, the lower polarizability of fluorine versus hydrogen lowers the cohesive energy of fluorocarbon chains as compared to their hydrogenated analogues. The two types of moieties also show different affinities: fluorocarbon chains are not only hydrophobic but also lipophobic, while hydrocarbon chains are both hydrophobic and fluorophobic.^[1] The combination of these two immiscible moieties imparts an amphiphilic character to *FnHm* diblocks. The latter self-assemble into micelles in both fluorocarbon and hydrocarbon solvents^[2,4] and form stable Langmuir monolayers at the air/water interface although they are devoid of hydrophilic moiety.^[1] It has been shown that *FnHm* monolayers consist of highly monodisperse, disk-like domains that form ordered hexagonal lattices.^[5] These domains have a diameter of $\Phi \approx 20\text{--}40 \text{ nm}$, which is an order of magnitude larger than the molecular length (2–3 nm). The formation of these mesoscopic domains was first revealed by atomic force microscopy (AFM) on transferred monolayers^[6] and later grazing incidence small-angle X-ray scattering (GISAXS) at the air/water interface.^[7] X-ray and neutron reflectivity studies demonstrated that the *FnHm* molecules are oriented vertically with the *F*-chains up while the *H*-chains are down and in contact with water,^[6,8–11] which is consistent with the higher hydrophobicity of fluoro-

[a] Dr. M. Veschgini,⁺ Dr. W. Abuillan,⁺ Dr. S. Inoue, S. Mielke, Prof. Dr. M. Tanaka
Physical Chemistry of Biosystems
Institute of Physical Chemistry, Heidelberg University
69120 Heidelberg (Germany)
E-mail: tanaka@uni-heidelberg.de

[b] Dr. A. Yamamoto, Prof. Dr. M. Tanaka
Institute for Integrated Cell-Material Sciences (iCeMS)
Kyoto University
Kyoto 606–8501 (Japan)

[c] X. Liu, Prof. Dr. M. P. Krafft
Institut Charles Sadron (CNRS UPR 22)
University of Strasbourg
23 rue du Loess, 67034 Strasbourg Cedex 2 (France)
E-mail: krafft@unistra.fr

[d] Dr. O. Konovalov
European Synchrotron Radiation Facility (ESRF) 71 avenue des Martyrs
Grenoble Cedex 9 38043 (France)

[e] Dr. S. Inoue
Present address: Kao company
1334 Minato, Wakayama, Wakayama Prefecture 640–8580 (Japan)

[†] These Authors contributed equally to this work.

[**] GISAXS: Grazing Incidence Small-Angle X-ray Scattering

Supporting Information for this article can be found under:
<https://doi.org/10.1002/cphc.201700325>.

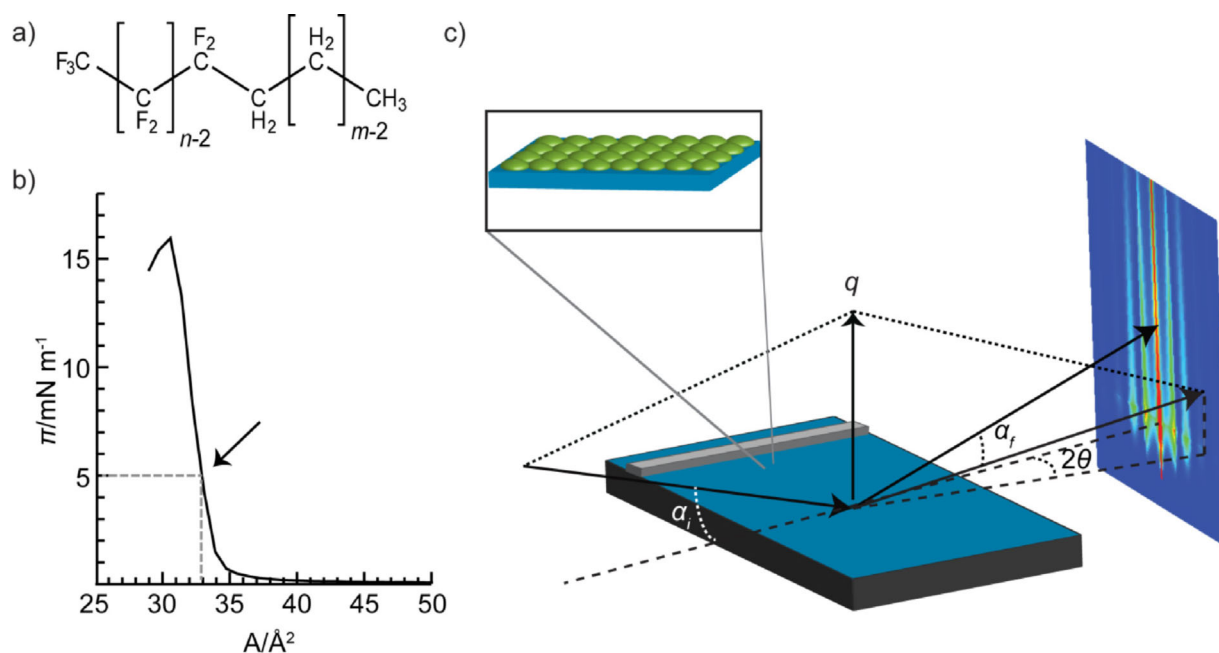


Figure 1. a) Chemical structure of the F_nH_m diblocks used in this study, b) typical pressure-area isotherm of a $F10H16$ monolayer recorded at the air/water interface. GISAXS experiments were performed at a constant surface pressure $\pi = 5 \text{ mN m}^{-1}$ (arrow). c) Schematic illustration of the experimental setup.

carbon chains. This molecular orientation was also supported by surface potential measurements on Langmuir monolayers, revealing a negative surface potential.^[12–14] However, an anti-parallel conformation for F_nH_m diblocks^[15] and the formation of a smectic bilayer^[16] have been proposed, too. Disk-like and striped surface domains were also reported for partially fluorinated carboxylic acids^[17] and partially fluorinated diether glycerols,^[18] respectively. Surface domains of various shapes were also published for combinations of fluorinated amphiphiles (phosphates, diethyl glycerols) with hydrocarbon and fluorocarbon oils^[19] or phospholipids.^[20–21]

Since F_nH_m domains can be transferred onto solid substrates even at a very low surface pressure $\pi \approx 0 \text{ mN m}^{-1}$,^[22] it was suggested that the self-assembly of the F_nH_m is dependent on surface concentration but not on surface pressure. Previous studies have demonstrated that the ratio between F_n and H_m segments influences the collapse pressure of the F_nH_m monolayer^[12–14] and modulates the domain size.^[8, 23–24] However, it should be noted that most of these studies are AFM studies that deal with monolayers transferred onto solid substrates, which may interfere with the initial structure. Except the study by Bardin et al.^[23], there have been no studies shedding light on the impact of H_m segment length on the surface domain structures at the air/water interface.

In this study, the structure of F_nH_m monolayers at the air/water interface was investigated using GISAXS (Figure 1) while systematically varying the lengths of the F_n and H_m blocks. In contrast to the previous studies focusing on the lattice parameters of F_nH_m domains,^[23] we performed the full calculation of form factor $F(q_y)$ and structure factor $S(q_y)$. These factors allowed direct determination of the diameter, height, and extent of lateral correlation between F_nH_m domains.

2. Results and Discussion

Figure 2a shows the scattering pattern of a $F10H16$ monolayer recorded at $\pi = 5 \text{ mN m}^{-1}$ as a representative example of two-dimensional reciprocal space map. The dark rectangular region near $q_y = 0$ represents the beam stop for the direct beam. The maximum scattering intensity is observed at $q_z \approx 0.28 \text{ nm}^{-1}$ (Yoneda peak), which decays rapidly by increasing q_z , reaching a plateau at $q_z \approx 0.4 \text{ nm}^{-1}$ (Figure S1). This extended rod-like scattering patterns indicate that the interfacial films of F_nH_m are composed of a monolayer with a two dimensional lattice of highly correlated nano-domains.^[7, 23, 25–26] Figure 2b represents the intensity profile along q_y . To improve the statistics, the intensity profile was obtained by integrating the scattering intensity between $q_z = 0.7$ and 0.9 nm^{-1} (red lines in Figure 2a). This region was chosen in order to exclude artifacts from the beam stop.

The scattering function $I(q_y)$, collected by GISAXS is given by the combination of the structure factor $S(q_y)$ and the form factor $F(q_y)$ according to [Eq. (1)]:

$$I(q_y) = A \times |F(q_y)|^2 \times S(q_y) \quad (1)$$

where A is a scaling factor. $F(q_y)$ accounts for the shape and size of the objects, while $S(q_y)$ reflects their lateral organization. In this study, we selected $F(q_y)$ of an oblate hemispheroid with a diameter Φ and height H (inset, Figure 2b and equation S2) based on previous AFM studies.^[5–6] The choice of the form factor was verified by comparing χ^2 values with other models, such as faceted sphere (Figure S3). The best fit obtained by the latter model exhibited a 2.5 times larger χ^2 . The form

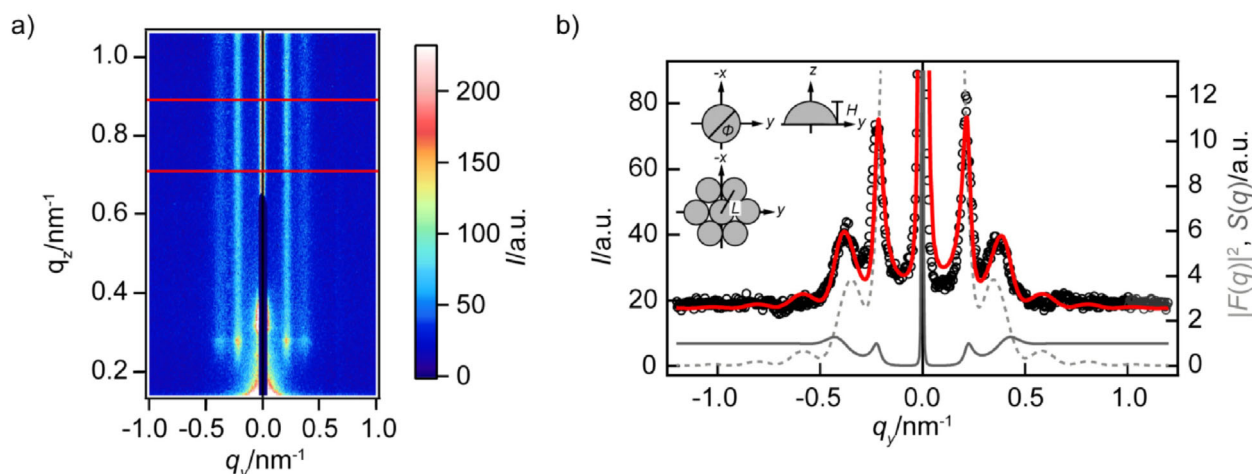


Figure 2. GISAXS signals from a *F10H16* monolayer at the air/water interface measured at $\pi = 5 \text{ mN m}^{-1}$. a) Two-dimensional detector readouts and b) intensity profile along q_y , integrated between the two red lines indicated in panel (a). The measured GISAXS signals (black open circles) were fitted by the combination of structure factor (solid gray line) and form factor (broken gray line). The best combined fit is presented by a red line. The top and side views of an oblate hemispheroid as well as the lattice model used for the fit are shown in an inset.

factor was considered within the framework of the distorted wave Born approximation (DWBA) in order to take the multiple scattering events into account.^[27–30] The structure factor $S(q_y)$ was modeled by a two dimensional hexagonal lattice with a lattice parameter L within the framework of the paracrystal theory (inset, Figure 2b and equation S4).^[31] This model was chosen based on previous AFM and X-ray scattering studies,^[6–7,22–25] and shows excellent agreement with the relative positions of the scattering peaks. It should be noted that the best fit could not be obtained by considering only the form factor. As shown in Figure 2b, the impact of the structure factor on the scattering intensity profile cannot be neglected.

The GISAXS analysis suggests that a *F10H16* domain has a diameter $\Phi = 30 \pm 5 \text{ nm}$ and a height $H = 4.9 \pm 0.9 \text{ nm}$. The calculated lattice parameter of the domains at the air/water interface is identical to the domain's diameter, indicating that the domains are tightly packed in a hexagonal lattice.

To further understand the influence of the *F*- and *H*-block length on the mesoscopic structure of the surface domains, the monolayers of various *F_nH_m* diblocks were characterized by GISAXS at $\pi = 5 \text{ mN m}^{-1}$. In a first step, we systematically varied the fluorocarbon chain length ($n = 8, 10$ and 12), while keeping the hydrocarbon chain length constant, $m = 16$. Figure 3 shows the integrated GISAXS signals from *F8H16* (Figure 3a) and *F12H16* (Figure 3b) monolayers. The solid and broken gray lines coincide with $S(q_y)$ and $F(q_y)$, respectively, and the red lines are the combined fitting curves. It should be noted that the selected models reproduce the experimental data very well.

$\Phi_{F8H16} = 29 \pm 5 \text{ nm}$, $\Phi_{F10H16} = 30 \pm 5 \text{ nm}$ and $\Phi_{F12H16} = 33 \pm 5 \text{ nm}$. Following the elongation of the *F_n* segments, the height of the hemispheroidal domains also increases; $H_{F8H16} = 3.8 \pm 0.7 \text{ nm}$, $H_{F10H16} = 4.9 \pm 0.9 \text{ nm}$, and $H_{F12H16} = 6 \pm 1 \text{ nm}$.

Figure 4 represents the integrated GISAXS signals corresponding to the hydrocarbon chain length ($m = 14, 16, 18$ and 20), while keeping the fluorocarbon chain length constant ($n =$

8). As for Figure 2b and Figure 3, the combined model (red curves) and the experimental data (symbols) exhibit excellent agreement, validating the models of $S(q_y)$ and $F(q_y)$ in this study. The elongation of the *H_m* segment from $m = 14$ to 20 results in a monotonic increase in the domain size from

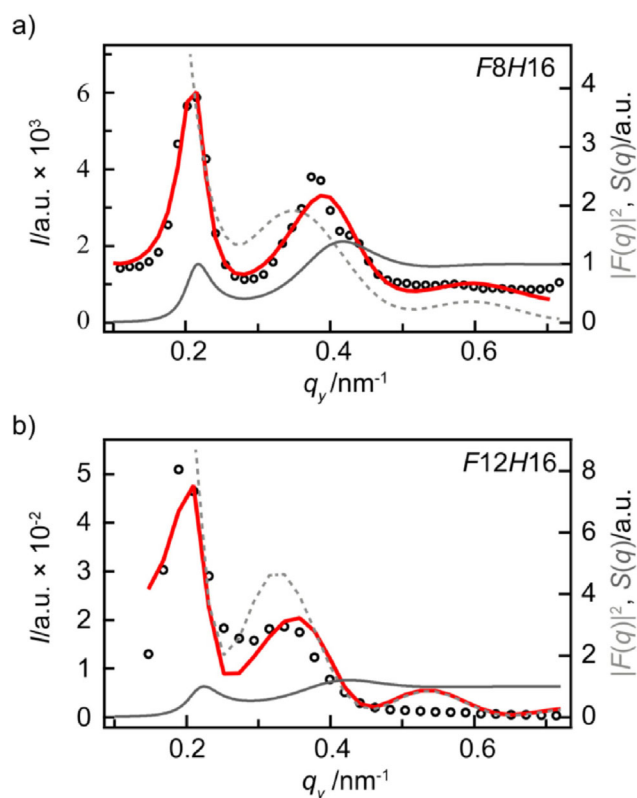


Figure 3. Integrated GISAXS signals (open black circles) and best fits (red curves) for a) *F8H16* and b) *F12H16* monolayers measured at $\pi = 5 \text{ mN m}^{-1}$. Solid and broken gray lines correspond to the structure factor $S(q_y)$ and form factor $|F(q_y)|^2$, respectively.

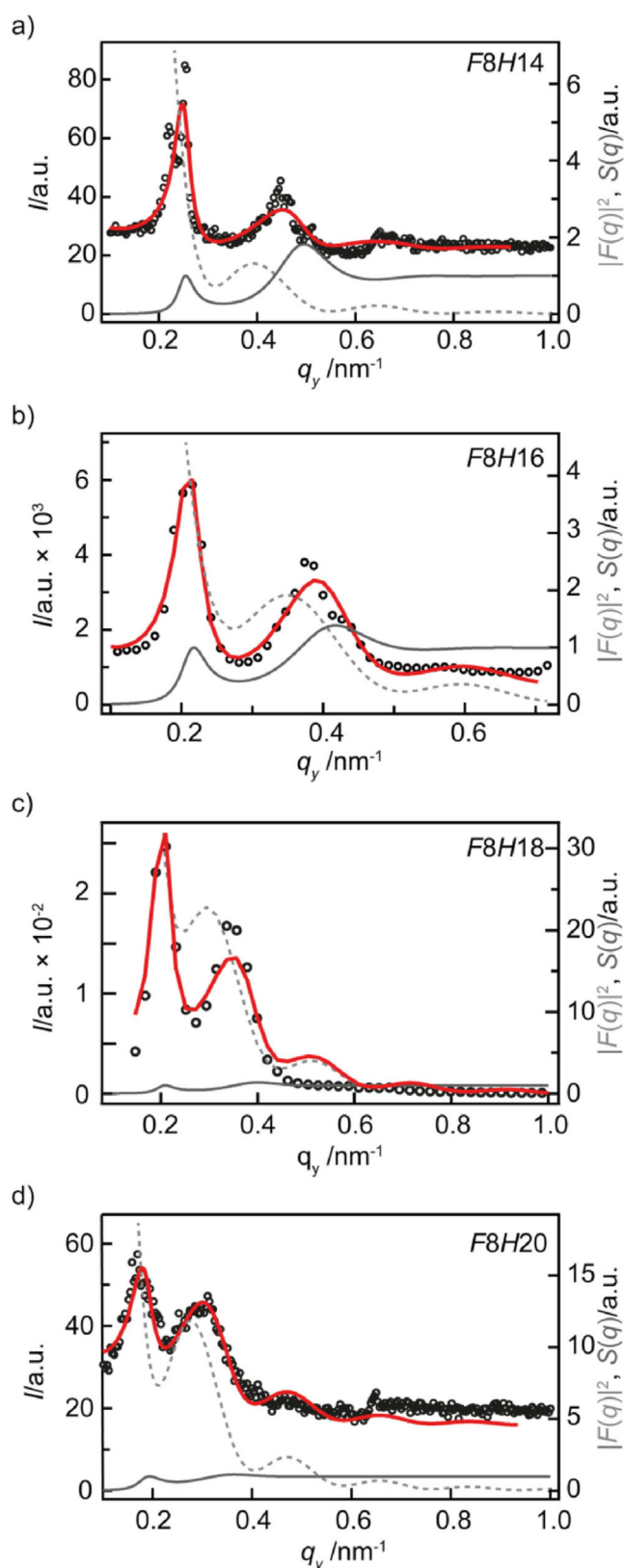


Figure 4. Integrated GISAXS signals (open black circles) and best fits (red curves) for a) *F8H14*, b) *F8H16*, c) *F8H18*, and d) *F8H20* monolayers measured at $\pi = 5 \text{ mN m}^{-1}$. Solid dark and broken light and gray lines correspond to the structure factor $S(q_y)$ and form factor $|F(q_y)|^2$, respectively.

$\Phi_{F8H14} = 28 \pm 4 \text{ nm}$ to $\Phi_{F8H20} = 36 \pm 7 \text{ nm}$. On the other hand, the height of the domains remains constant at $H \approx 3.6 \pm 0.6 \text{ nm}$ for $m = 14, 16$, and 18 , suggesting that the hydrocarbon chains cannot adopt an ordered *all-trans* conformation due to the steric constrain exerted by the bulky fluorocarbon chains. It is notable that *F8H20* domains are much thicker ($H_{F8H20} = 6.1 \pm 1.2 \text{ nm}$) than the domains of the other *F8Hm* diblocks, suggesting that *F8H20* molecules might form a different type of surface domains due to stronger cohesion between *Hm* segments.

2.1. Influence of Block Lengths on Domain Size

Figure 5 summarizes the change in the diameter of the surface domains (black) as a function of fluorocarbon chain length, n (Figure 5a) and hydrocarbon chain length m (Figure 5b). As summarized in Table S5, the calculated domain sizes agree well with those reported in previous GISAXS studies.^[7,23] However, it should be noted that these former studies solely relied on the position of the GISAXS peaks, and used the lattice parameters to determine the domain size. In general, such an approach might cause an overestimation of the domain size, when domains are not tightly packed in a hexagonal lattice. Especially, this strategy is not applicable when the domains of ordered small molecules are diluted in a disordered matrix.

A more efficient alternative approach is to measure grazing-incidence X-ray diffraction at wide angle, and to determine the size S of the crystallites, that is, the coherence length, according to the Scherrer equation [Eq. (2)]:

$$S \approx 0.9 \times 2\pi \sqrt{(FWHM)^2 - (\Delta q_y)^2} \quad (2)$$

where FWHM is the full width at half maximum of the wide-angle diffraction peak and Δq_y the angular resolution of the detector.^[21] In case a domain consists of a single crystallite, the domain size Φ corresponds to the coherence length S and can be calculated from the width of the wide angle diffraction peak using equation 2.^[21] However, the previous GID analysis^[23] yielded a coherence length of 2–5 nm for *F8Hm* ($m = 16, 18, 20$), suggesting that a domain of *F8Hm* is not composed of one single crystallite. Therefore, in this study we performed the full calculation of structure factor $S(q_y)$ and form factor $F(q_y)$ of mesoscopic domains of organic surfactants self-assembled at the air/water interface for the first time, and calculated the domain size from $F(q_y)$.

The equilibrium domain radius is governed by the balance between i) the line tension λ , which tends to minimize the domain's boundary length and ii) the repulsive dipole-dipole interaction between the molecules within the domain.^[32] McConnell suggested the equilibrium domain radius to be $R_{eq} \propto \exp(\lambda/\mu^2)$, where μ is the difference in dipole density between the domain and its surrounding phase.^[32] Since the dipole moment of *F_nH_m* molecules is mainly determined by their terminal CF_3 group and the $\text{CF}_2\text{-CH}_2$ junction between their hydro- and fluorocarbon blocks, it is expected to be independent from the molecular length, which was supported by semi-

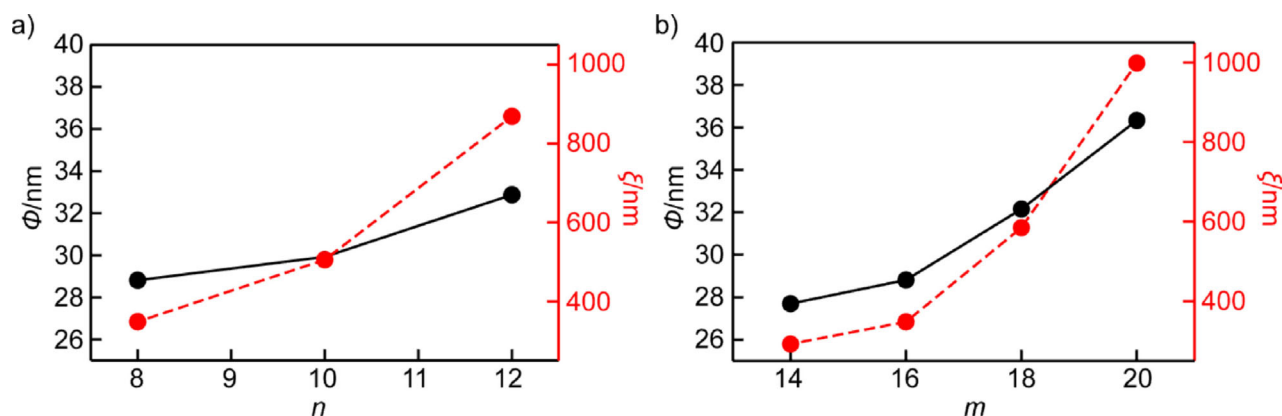


Figure 5. Calculated domain diameter Φ (black) and correlation length ξ (red) as a function of a) fluorocarbon block length (F_nH_{16} ; $n=8, 10,$ and 12) and b) hydrocarbon block length (F_8H_m ; $m=14, 16, 18,$ and 20).

empirical calculations as well as by surface potential measurements.^[12,33] Therefore, the increase in domain size with increasing hydrocarbon and fluorocarbon chain lengths can be attributed to an increase in the line tension due to the increase in attractive van der Waals interactions. In addition, the less pronounced impact of the F -chain length on domain size might be ascribed to the lower polarizability of fluorocarbon compared to hydrocarbon chains.

2.2. Influence of Block Lengths on Lateral Correlation

In addition to the analysis mentioned above, the calculation of radial distribution functions allows for the precise estimation of how far the correlation between particles extends through many particle interactions. Since the structure factor can be considered as the Fourier transformation of the real space pair correlation function $g(r)$, this can be used to determine the correlation length ξ within the framework of the short-range order (SRO) model [Eq. (3)].^[34–35]

$$\xi = \langle d \rangle^3 / (2\sigma^2) \quad (3)$$

where $\langle d \rangle$ represents the mean distance between two adjacent domains, which corresponds to the diameter Φ of the surface domains. σ describes the root mean square standard deviation of $\langle d \rangle$ that coincides with the width of the first correlation peak in $g(r)$.^[34] As presented in Figure 5a (red), the correlation length of F_nH_{16} at $\pi=5$ mN m⁻¹ monotonically increases from $\xi_{F_8H_{16}} \approx 350$ nm to $\xi_{F_{12}H_{16}} \approx 870$ nm according to the elongation of the F_n segment. The same tendency is found for F_8H_m molecules (Figure 5b, red), where the correlation increases from $\xi_{F_8H_{14}} \approx 300$ nm to $\xi_{F_8H_{20}} \approx 1000$ nm, following the elongation of the H_m segment. These values are distinctly larger than the correlation lengths previously reported for F_8H_m , $\xi \approx 175$ – 215 nm.^[23] In the latter account, ξ was calculated from the width of the scattering peak using the Scherrer equation (so-called “long-range order model” in which the structure factor exhibits a constant peak width). This analysis ignored the possible contribution of the form factor (gray broken lines,

Figure 3 and Figure 4), which may cause an underestimation of the correlation length.

In contrast, within the framework of the “short-range order model” that we introduced in the present study, the peak width of the structure factor $S(q_y)$ becomes larger with increasing q_y , and accordingly the peak width of the pair correlation function. Therefore, the Fourier transformation of $S(q_y)$ used here allows for a more precise determination of the correlation length ξ . The comparison of the values calculated in this study with those from the previous account are presented in the Supporting Information (Table S5). To further highlight the impact of the hydrocarbon or fluorocarbon chain lengths on the lateral packing order of the F_nH_m domains, we normalized the correlation length ξ by the domain diameter Φ (Figure 6). The normalized correlation length ξ/Φ exhibits two clear characteristic features. First, for all the F_nH_m molecules investigated, the lateral correlation between the domains can reach distances over 10–26 times longer than a single domain size, implying that mesoscopic domains of F_nH_m are strongly correlated at the air/water interface. The normalized correlation length

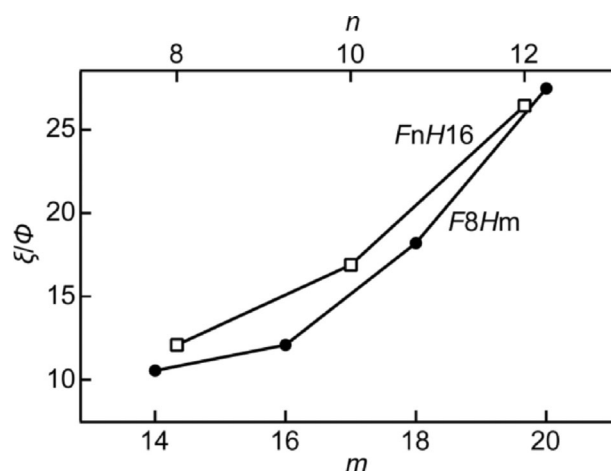


Figure 6. Correlation length ξ normalized by surface domain diameter Φ as a function of the hydrocarbon block length m (solid circles, F_8H_m) and fluorocarbon block length n (open squares, F_nH_{16}).

of $FnHm$ is distinctly larger than that reported for the domains of perfluorinated surfactants in phospholipid matrices, which correspond to $\xi/\Phi = 3\text{--}4$.^[21] Second, the elongation of the chains leads to a monotonic increase in ξ/Φ , suggesting that the increase in correlation length ξ is not only caused by the increase in size Φ . This finding indicates that the larger the domains are, the stronger the inter-domain repulsion becomes.

It is noteworthy that previous AFM studies on $FnHm$ diblocks monolayers transferred onto silicon wafers showed the presence of elongated, worm-like micelles together with circular domains.^[24] The fraction and length of these elongated micelles were reported to increase with the molecular length and to decrease with increasing surface pressure. This suggests that the correlation length should decrease with increasing block length which is in contrast to our findings. To further verify whether the elongated micelles are present at the air/water interface, we also compared the scattering patterns of $F10H16$ at $\pi = 2\text{ mN m}^{-1}$ and 10 mN m^{-1} (Figure S6). For this compound, Zhang et al. reported a decrease in the area fraction of elongated micelles from $\approx 10\%$ at $\pi = 2\text{ mN m}^{-1}$ to $\approx 1.5\%$ at $\pi = 10\text{ mN m}^{-1}$.^[8,24] However, we found that the scattering pattern did not show any significant change of the width of the first peak and hence of the degree of lateral order. Hence, as previously suggested^[23], it is possible that the formation of elongated micelles is an artifact from the transfer of monolayers onto silicon substrates. Changes in molecular conformational order upon transfer of monolayers onto a solid substrate have been reported for partially fluorinated fatty acids.^[36]

2.3. "Deformability" of Surface Micelles

The strong correlation of uniform $FnHm$ domains suggests that they resist against deformation and avoid coalescence. In fact, the pressure-area isotherms of $FnHm$ monolayers (Supporting Information, Figure S7) clearly show that $FnHm$ monolayers are very poorly compressible. The lateral compressibility of $FnHm$ monolayers calculated from pressure-area isotherms, $\kappa^{-1} = -(1/A)(\partial A/\partial \pi) \approx 10\text{ mN}$ at $\pi = 5\text{ mN m}^{-1}$, is comparable to that of a liquid condensed phase of fatty acids, $\kappa^{-1} \approx 4\text{--}10\text{ mN}$.^[37] Figure 7 shows the diameter of domains Φ calculated from GISAXS signals measured at difference surface pressures π . The domain size of both $FnH16$ (Figure 7a) and $F8Hm$ (Figure 7b) does not decrease significantly when surface pressure increases. The same tendency is observed for $F10Hm$ (Figure S8). When the lattice parameter L (inter-domain distance) calculated from the structure factor $S(q_y)$ is normalized by its own diameter Φ , the L/Φ ratio calculated for all the domains remains at 0.8–1.0 at $\pi > 0\text{ mN m}^{-1}$. This finding implies that $FnHm$ domains are not deformed during monolayer compression and retain their initial shape. These results indicate that the formation of highly ordered hexagonal lattices originates from the repulsive interactions between $FnHm$ domains, which reach up to distances 26 times larger than the domain's diameter.

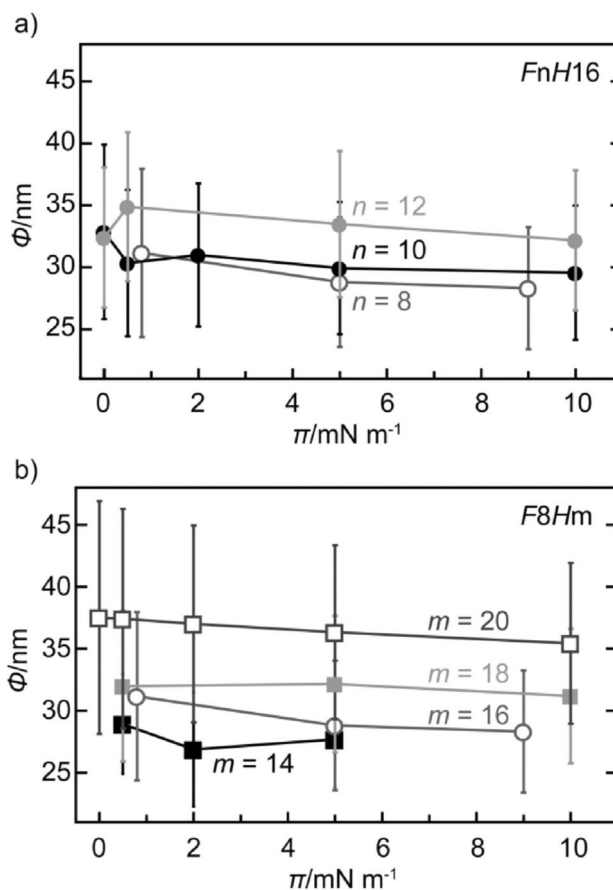


Figure 7. Influence of surface pressure π on domain diameter Φ , summarized for a) $FnH16$ ($n = 8, 10,$ and 12) and b) $F8Hm$ ($m = 14, 16, 18,$ and 20).

3. Conclusions

Semi-fluorinated diblocks $FnHm$ self-assemble into highly monodisperse, circular domains. In this study, full calculation of GISAXS signals collected at the air/water interface, allowed direct and precise quantitative determination of the structure and form factors, and hence, the impact of the block lengths on the size, shape, and lateral correlation.

The increase in Hm segment length leads to a monotonic increase in domain diameter Φ , for example, $\Phi_{F8H14} = 28\text{ nm}$ and $\Phi_{F8H20} = 36\text{ nm}$. The same tendency was observed when the Fn segment length was increased, for example, $\Phi_{F8H16} = 29\text{ nm}$ and $\Phi_{F12H16} = 33\text{ nm}$. The increase in surface domain diameter is attributed to an increase in the line tension caused by the increase in attractive van der Waals interactions between longer hydro- and fluorocarbon blocks.

Moreover, the pair correlation function $g(r)$ in real space was deduced from the structure factor $S(q_y)$ in order to calculate the inter-domain correlation lengths ξ . The results revealed a high degree of spatial correlation of the $FnHm$ domains, for which lateral correlation can reach a distance that is 10–26 times larger than the domain size. Moreover, the increase in Fn and Hm segment length leads to a monotonic increase in ξ/Φ ratio. Last but not least, we found that the diameter of the $FnHm$ domains remains almost constant independently of sur-

face pressure π , implying that the *FnHm* domains can resist deformation due to the strong repulsive inter-domain interactions.

Our results demonstrate the large potential of the full GISAXS calculation approach in structural studies of mesoscopic domains of organic molecules. This approach can be utilized to monitor the fine-tuning of hierarchical structural correlation from molecular structures to domain formation, and to lateral correlation between domains, for which length scales can span almost three orders of magnitude.

Experimental Section

Materials: The compounds tested in this study: *F8H14*, *F8H16*, *F8H18*, *F8H20*, *F10H16*, *F10H18* and *F12H16* were synthesized according to^[38] and purified by repeated crystallizations from methanol. Chemical purity (>99%) was determined by TLC, NMR, elemental analysis and MALDI-TOF mass spectrometry. Double deionized water (MilliQ, Molsheim) with a specific resistivity $\rho > 18 \text{ M}\Omega \text{ cm}$ was used throughout this study.

GISAXS: The experiments were performed at the beam line ID10 of the European Synchrotron Radiation Facility (ESRF, Grenoble, France). The monolayers were prepared by spreading 150 μl of a 1 mm solution of *FnHm* in CHCl_3 onto the water surface of a Langmuir film balance (surface area $\approx 692 \text{ cm}^2$) equipped with a movable barrier. The trough was enclosed in a gastight box and all experiments were performed in a helium atmosphere at $T = 293 \text{ K}$. After evaporation of the solvent (>20 min), the monolayer was compressed at a speed of $\approx 35 \text{ mm}^2 \text{ s}^{-1}$ to a surface pressure of $\pi = 5 \text{ mN m}^{-1}$ which was kept constant during GISAXS experiments. A typical pressure-area isotherm of a monolayer of *F10H16* is shown in Figure 1 b, while those of the other *FnHm* compounds are shown in Figure S7. A monochromatic X-ray beam of 10 keV impinged the interface at an incident angle of $\alpha_i = 0.2^\circ$ or at an energy of 8 keV and $\alpha_i = 0.12^\circ$ near the critical angle of total external reflection. The geometry of the GISAXS experiment is illustrated in Figure 1 c. The scattering intensity was detected using a 2D-pixel detector (MaxiPix). The background scattering was measured on a pure water subphase. After background subtraction, the scattering patterns were analyzed using the FitGISAXS software^[39] on the IGOR PRO platform (WaveMetrics, Portland, USA). The scattering profile along q_y was averaged over a range $q_z = (0.8 \pm 0.1) \text{ nm}^{-1}$. The obtained scattering intensity profiles were fitted within the distorted wave Born approximation using the implemented functions for a hexagonal paracrystal of monodisperse oblate hemispheroids as a model for the *FnHm* monolayers. Structure factors $S(q_y)$ and form factors $F(q_y)$ were obtained from the best fit by stepwise optimizing the fitting parameters: background intensity, scaling factor A [Equation (1)], hemispheroid diameter Φ , standard deviation of the Φ , the ratio H/Φ , where H represents the hemispheroid height and the ratio L/Φ , where L corresponds to the lattice constant. The final fit was obtained by letting all parameters float.

Acknowledgements

We thank ESRF for the synchrotron radiation beam time. We thank the French Research Agency (grant ANR-14-CE35-0028-01 to M.P.K.), the German Science Foundation (DFG Ta259/12 to M.T.), and the Japan Society for the Promotion of Science

(16K05515 to A.Y.). M.V. thanks DFG (GRK1114, EcTop2) for the fellowship. S.M. is thankful to Konrad-Adenauer Foundation and X.L. thanks ANR for PhD fellowships. W.A. thanks Dr. D. Babonneau for insightful suggestions. M.T. is an investigator of the German Excellence Cluster "CellNetworks". iCeMS is supported by World Premier International Research Center Initiative (WPI), MEXT, Japan.

Conflict of interest

The authors declare no conflict of interest.

Keywords: air/water interface • GISAXS • hierarchical self-assembly • nano-domains • semi-fluorinated alkanes

- [1] M. P. Krafft, J. G. Riess, *Chem. Rev.* **2009**, *109*, 1714–1792.
- [2] M. Broniatowski, P. Dynarowicz-Łątka, *Adv. Colloid Interface Sci.* **2008**, *138*, 63–83.
- [3] C. W. Bunn, E. R. Howells, *Nature* **1954**, *174*, 549–551.
- [4] M. P. Turberg, J. E. Brady, *J. Am. Chem. Soc.* **1988**, *110*, 7797–7801.
- [5] M. P. Krafft, *Acc. Chem. Res.* **2012**, *45*, 514–524.
- [6] M. Maaloum, P. Muller, M. P. Krafft, *Angew. Chem. Int. Ed.* **2002**, *41*, 4331–4334; *Angew. Chem.* **2002**, *114*, 4507–4510.
- [7] P. Fontaine, M. Goldmann, P. Muller, M.-C. Fauré, O. Konovalov, M. P. Krafft, *J. Am. Chem. Soc.* **2005**, *127*, 512–513.
- [8] G. Zhang, M. Maaloum, P. Muller, N. Benoit, M. P. Krafft, *Phys. Chem. Chem. Phys.* **2004**, *6*, 1566–1569.
- [9] Z. Huang, A. A. Acero, N. Lei, S. A. Rice, Z. Zhang, M. L. Schlossman, *J. Chem. Soc. Faraday Trans.* **1996**, *92*, 545–552.
- [10] L. de Viguierie, R. Keller, U. Jonas, R. Berger, C. G. Clark, C. O. Klein, T. Geue, K. Müllen, H.-J. Butt, D. Vlassopoulos, *Langmuir* **2011**, *27*, 8776–8786.
- [11] A. Mourran, B. Tartsch, M. Gallyamov, S. Magonov, D. Lambreva, B. I. Ostrovskii, I. P. Dolbnya, W. H. de Jeu, M. Moeller, *Langmuir* **2005**, *21*, 2308–2316.
- [12] M. Broniatowski, I. Sandez Macho, J. Miñones, P. Dynarowicz-Łątka, *J. Phys. Chem. B* **2004**, *108*, 13403–13411.
- [13] M. Broniatowski, I. Sandez Macho, P. Dynarowicz-Łątka, *Thin Solid Films* **2005**, *493*, 249–257.
- [14] M. Broniatowski, J. Miñones Jr, P. Dynarowicz-Łątka, *J. Colloid Interface Sci.* **2004**, *279*, 552–558.
- [15] A. E. Abed, M. C. Fauré, E. Pouzet, O. Abillon, *Phys. Rev. E* **2002**, *65*, 051603.
- [16] A. El Abed, E. Pouzet, M. C. Fauré, M. Sanière, O. Abillon, *Phys. Rev. E* **2000**, *62*, R5895–R5898.
- [17] T. Kato, M. Kameyama, M. Ehara, K.-I. Iimura, *Langmuir* **1998**, *14*, 1786–1798.
- [18] M. F. Schneider, D. Andelman, M. Tanaka, *J. Chem. Phys.* **2005**, *122*, 094717.
- [19] S. Trabelsi, Z. Zhang, S. Zhang, T. R. Lee, D. K. Schwartz, *Langmuir* **2009**, *25*, 8056–8061.
- [20] C. Gege, M. F. Schneider, G. Schumacher, L. Limozin, U. Rothe, G. Bendas, M. Tanaka, R. R. Schmidt, *Chemphyschem* **2004**, *5*, 216–224.
- [21] J. Oelke, A. Pasc, A. Wixforth, O. Konovalov, M. Tanaka, *Appl. Phys. Lett.* **2008**, *93*, 213901.
- [22] A. Gonzalez-Perez, C. Contal, M. P. Krafft, *Soft Matter* **2007**, *3*, 191–193.
- [23] L. Bardin, M.-C. Fauré, D. Limagne, C. Chevillard, O. Konovalov, E. J. M. Filipe, G. Waton, M. P. Krafft, M. Goldmann, P. Fontaine, *Langmuir* **2011**, *27*, 13497–13505.
- [24] G. Zhang, P. Marie, M. Maaloum, P. Muller, N. Benoit, M. P. Krafft, *J. Am. Chem. Soc.* **2005**, *127*, 10412–10419.
- [25] P. Fontaine, M.-C. Fauré, L. Bardin, E. J. M. Filipe, M. Goldmann, *Langmuir* **2014**, *30*, 15193–15199.
- [26] A. Gibaud, S. Dourdain, O. Gang, B. M. Ocko, *Phys. Rev. B* **2004**, *70*, 161403.

- [27] J. B. He, Z. W. Niu, R. Tangirala, J. Y. Wan, X. Y. Wei, G. Kaur, Q. Wang, G. Jutz, A. Boker, B. Lee, S. V. Pingali, P. Thiyagarajan, T. Emrick, T. P. Russell, *Langmuir* **2009**, *25*, 4979–4987.
- [28] P. Busch, M. Rauscher, D. M. Smilgies, D. Posselt, C. M. Papadakis, *J. Appl. Crystallogr.* **2006**, *39*, 433–442.
- [29] M. Rauscher, T. Salditt, H. Spohn, *Phys. Rev. B* **1995**, *52*, 16855–16863.
- [30] S. K. Sinha, E. B. Sirota, S. Garoff, H. B. Stanley, *Phys. Rev. B* **1988**, *38*, 2297–2311.
- [31] R. Hosemann, S. N. Bagchi, *Acta Crystallographica* **1952**, *5*, 612–614.
- [32] H. M. McConnell, R. De Koker, *J. Phys. Chem.* **1992**, *96*, 7101–7103.
- [33] P. Dynarowicz Łatka, M. Pérez-Morales, E. Muñoz, M. Broniatowski, M. T. Martín-Romero, L. Camacho, *J. Phys. Chem. B* **2006**, *110*, 6095–6100.
- [34] M. Schmidbauer in *Dynamical Scattering Effects at Grazing Incidence Conditions*, Vol., Springer-Verlag Berlin Heidelberg, **2004**, pp. 127–138.
- [35] M. Schmidbauer, M. Hanke, R. Köhler, *Phys. Rev. B* **2005**, *71*, 115323.
- [36] Y. Ren, K.-i. Iimura, T. Kato, *J. Phys. Chem. B* **2002**, *106*, 1327–1333.
- [37] E. K. R. J. T. Davies, *Interfacial Phenomena*, Academic Press, New York, **1963**.
- [38] N. O. Brace, *J. Fluorine Chem.* **1999**, *93*, 1–25.
- [39] D. Babonneau, *J. Appl. Crystallogr.* **2010**, *43*, 929–936.

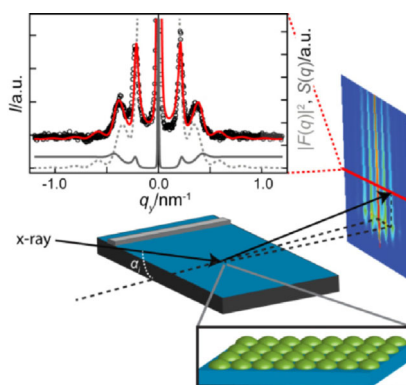
Manuscript received: March 27, 2017

Accepted manuscript online: May 12, 2017

Version of record online: ■ ■ ■ ■, 0000

ARTICLES

Hierarchical self-assembly: Semi-fluorinated alkanes (*FnHm*) self-assemble into highly monodisperse nano-domains at the air/water interface. Grazing incidence small angle X-ray scattering (GISAXS) is used to elucidate the mesoscopic structure of *FnHm* Langmuir monolayers. The full calculation of form and structure factors reveals the impact of the fluoro- and hydrocarbon block lengths on the size, shape and lateral organization of the nano-domains.



M. Veschgini, W. Abuillan, S. Inoue, A. Yamamoto, S. Mielke, X. Liu, O. Konovalov, M. P. Krafft, M. Tanaka**

■ ■ - ■ ■

Size, Shape, and Lateral Correlation of Highly Uniform, Mesoscopic, Self-Assembled Domains of Fluorocarbon-Hydrocarbon Diblocks at the Air/Water Interface: A GISAXS Study

